Voltage-controlled spin-wave Doppler shift in a ferromagnetic/ferroelectric heterojunction

Shaojie Hu,[1,*] Kang Wang,[2] Tai Min,[2,3] and Takashi Kimura[1]

[1] *Department of Physics, Kyushu University, 744 Motooka, Fukuoka 819-0395, Japan*

[2] *Center for Spintronics and Quantum Systems, State Key Laboratory for Mechanical Behavior of Materials, School of Materials Science and Engineering, Xi'an Jiaotong University, Xi'an, Shaanxi 710049, China*

[3] *School of Materials Science and Intelligent Engineering, Nanjing University, Suzhou 215163, China*

(Received 29 February 2024; revised 12 May 2024; accepted 12 July 2024; published 31 July 2024)

Efficient manipulation of spin waves (SWs) is considered as one of the promising means for encoding information with low power consumption in next-generation spintronic devices. The SW Doppler shift is a key phenomenon obtained by manipulating SW propagation. Here, we predict an efficient way to control the SW Doppler shift by voltage-control magnetic-anisotropy-boundary (MAB) movement in the FM-FE heterojunction. From the micromagnetic simulation, we verified that the SW Doppler shift aligns well with our theoretical predictions in $Fe/BaTiO_3$ heterostructure. The SW Doppler shift also shows an ultra-wide-band-shift (over 5 GHz) property with voltage. Such an efficient SW Doppler shift may provide one possible way to measure the Hawking radiation of an analogue black hole in the SW systems.

DOI: 10.1103/PhysRevApplied.22.014085

I. INTRODUCTION

Magnonics, a burgeoning field rooted in the exploration of quantum magnetic dynamic phenomena, is primarily dedicated to the in-depth research and practical application of spin waves (SWs). These SWs hold promise for advanced information processing at the nanoscale, potentially revolutionizing how we store and compute data with ultralow power consumption [1–7]. Efficiently controlling the spin-wave propagation offers a potential alternative for encoding information beyond CMOS computing due to their absence of Joule heating during propagation, scalability to atomic dimensions, and diverse nonlinear and nonreciprocal phenomena [8–11]. Much like sound or light waves, SWs inherently exhibit wave properties, including the Doppler effect that denotes frequency shifts due to relative motion between the source and observer. Recent studies have highlighted numerous innovative SW Doppler shift occurrences. Stancil *et al.* reported the experimental observation of an inverse Doppler shift from left-handed dipolar SWs with a moving pick-up antenna, which is the intrinsic characteristic of left-handed, or backward SWs [12]. Vlaminck and Bailleul found the current-induced SW Doppler shift that related to the adiabatic spin-transfer torque, which can be used as a probe of spin-polarized transport in various metallic ferromagnets [13]. The current-driven domain-wall motion could also induce a significant SW Doppler effect [14]. Meanwhile, Yu *et al.* predicted the SW Doppler shift by magnon drag in magnetic insulators [15]. In parallel, Nakane and Kohno studied the current-induced SW Doppler shift in antiferromagnets [16]. So, researchers have hypothesized that it is possible to create magnonic black-hole and white-hole horizons using an efficient method involving spin current-driven SW Doppler shifts. This means that the SW Doppler shift might not provide only a mechanism for simulating gravitational phenomena, but also offer a way to study analogue gravity and even measure the Hawking radiation emitted by an analogous black hole [17,18]. The intriguing nature of these phenomena has significantly heightened research interest in the SW Doppler shift, pushing scientists and scholars to delve deeper into its intricacies and potential applications.

So far, the preponderance of investigations into the SW Doppler shift has been concentrated on individual ferromagnetic materials that are modulated through electric current control. Such a constrained approach inadvertently poses limitations on realizing the aspirational goal of ultralow power consumption, which is pivotal for the nuanced manipulation of SWs. Compounding this challenge, it has been observed that the SW Doppler shift frequencies are consistently far from the GHz benchmark. In the broader academic discourse, the magnetoelectric effect emerges as a promising avenue, widely regarded for its efficacy in directing the propagation of SWs [19–24]. This is achieved with a commendable reduction in power consumption, especially when deployed within multiferroic materials. In the pantheon of multiferroic systems,

*Contact author: hu.shaojie@phys.kyushu-u.ac.jp, shaojie.hu.zzu@gmail.com

 © 2024 American Physical Society

the artificial ferromagnetic/ferroelectric (FM-FE) heterojunction stands as an archetypal representative [25–33]. Within this context, we present a pronounced SW Doppler shift attributed to the motion of the magnetic anisotropy boundary (MAB) inherent in the FM-FE heterojunction, a process which is deftly modulated by voltage.

Figure 1 provides a schematic representation of SW Doppler shift precipitated by the voltage-controlled MAB movement in FM-FE heterojunction. Within this configuration, the ferromagnetic layer, positioned atop a ferroelectric substrate with both in-plane and out-of-plane polarized domains, manifests two distinct magnetic anisotropy regions: A1 and A2. Varied magnetic anisotropies result from the strain-induced inverse magnetostriction effect across distinct polarized domains [34]. The MAB separating the two magnetic anisotropy regions is pinned on the ferroelectric domain wall and parallel to y axis. A positive (negative) voltage-controlled perpendicular electric field can drive the motion of the ferroelectric domain wall along x ($-x$) axis as well as the MAB [35]. The frequencies of reflected and transmitted SWs will show the red or blue shift by moving MAB. This letter presents an analytical model of the SW Doppler shift, which is further validated through magnetic simulation.

For simplicity, we assume that the MAB moves at a constant velocity v_{MAB}. The incident SW propagates along the x axis and perpendicular to the MAB. In the observer's system S, which is stationary with respect to the lab frame,

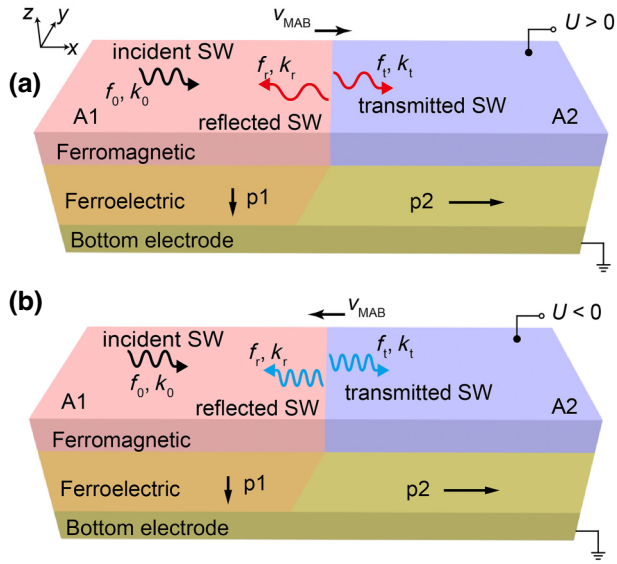

FIG. 1. The schematic of SW Doppler shift induced by the voltage-controlled MAB movement in FM-FE heterojunction. The out-of-plane and in-plane polarization domains in the ferroelectric layer transfer different strains to the ferromagnetic layer. The ferromagnetic layer exhibits different anisotropy regions owing to inverse magnetostriction. (a) One case of SW Doppler red shift caused by a positive voltage. (b) One case of SW Doppler blue shift caused by a negative voltage.

the general dispersion relations of SWs in A1 and A2 are described as different functions $f_1 = F_1(\mathbf{k})$ and $f_2 = F_2(\mathbf{k})$ with wave vector $\mathbf{k}$. In the moving system S', which is stationary with respect to the MAB, the dispersion functions $f_1' = F_1'(\mathbf{k})$ and $f_2' = F_2'(\mathbf{k})$ with vector $\mathbf{k}'$ in A1 and A2 are given as follows by Lorentz transformation:

$$f'_{i=1,2} = F'_{i=1,2}(\mathbf{k}') = \Gamma\left(F_{i=1,2}(\mathbf{k}') - \frac{\mathbf{k}'\cdot\mathbf{v}_{\mathrm{MAB}}}{2\pi}\right),$$
$$\mathbf{k}'_{i=1,2} = \Gamma\left(\mathbf{k}_{i=1,2} - \frac{2\pi f_{i=1,2}\mathbf{v}_{\mathrm{MAB}}}{c^2}\right), \quad (1)$$

where $\Gamma = \left(1 - v_{\mathrm{MAB}}^2/s^2\right)^{-1/2}$ [36,37], $s = \gamma\sqrt{A_{\mathrm{ex}}H_{\mathrm{ex}}/M_{\mathrm{s}}}$ is the limited group velocity of spin waves in ferromagnet, where γ is the gyromagnetic ratio, A_{ex} is exchange constant of the ferromagnet, H_{ex} stands for the exchange field that keeps magnetic sublattices parallel [38–42]. Under the limitation of $v_{\mathrm{MAB}} \ll s$, the f' and $\mathbf{k}'$ can be written as follows:

$$f'_{i=1,2} = F'_{i=1,2}(\mathbf{k}') \approx F_{i=1,2}(\mathbf{k}') - \frac{\mathbf{k}'\cdot\mathbf{v}_{\mathrm{MAB}}}{2\pi}, \mathbf{k}'_{i=1,2} \approx \mathbf{k}_{i=1,2}. \quad (2)$$

The frequencies and wave vectors of incident, reflected, and transmitted SWs in system S and S' are defined as f_0, $\mathbf{k_0}$, f_{r}, $\mathbf{k}_{\mathrm{r}}$, f_{t}, $\mathbf{k}_{\mathrm{t}}$, f_0', $\mathbf{k}_0'$, f_{r}', $\mathbf{k}_{\mathrm{r}}'$, f_{t}' and $\mathbf{k}_{\mathrm{t}}'$, respectively. If the incident SW from the A1 region propagates to A2, as shown in Fig. 1, the frequencies of reflected and transmitted SWs in system S can be derived under the limitation of $v_{\mathrm{MAB}} \ll s$ as follows:

$$f_{\mathrm{r}} = \Gamma\left(f_{\mathrm{r}}' + \frac{\mathbf{k}_{\mathrm{r}}'\cdot\mathbf{v}_{\mathrm{MAB}}}{2\pi}\right)$$
$$\approx f_0 - (\mathbf{k}_0 - \mathbf{k}_{\mathrm{r}}')\cdot\frac{\mathbf{v}_{\mathrm{MAB}}}{2\pi}, \quad (3)$$
$$f_{\mathrm{t}} = \Gamma\left(f_{\mathrm{t}}' + \frac{\mathbf{k}_{\mathrm{t}}'\cdot\mathbf{v}_{\mathrm{MAB}}}{2\pi}\right)$$
$$\approx f_0 - (\mathbf{k}_0 - \mathbf{k}_{\mathrm{t}}')\cdot\frac{\mathbf{v}_{\mathrm{MAB}}}{2\pi}, \quad (4)$$

where incident frequency f_0 is known, $\mathbf{k}_0$ can be obtained from the dispersion relation of SWs in the incident region. $\mathbf{k}_{\mathrm{r}}'$ and $\mathbf{k}_{\mathrm{t}}'$ can be obtained from Eq. (2), respectively. So the frequency shift of the SW Doppler effect is dominated by the second terms of Eqs. (3) and (4), which not only relate to the velocity of MAB but also the deviation of the incident and reflected (or transmitted) wave vectors determined by different magnetic anisotropy.

To validate such SW Doppler shift, we conducted the micromagnetic simulation in a well-built artificial multiferroic system Fe/$BaTiO_3$ [43,44] by using the GPU-accelerated micromagnetic software Mumax3 [45].

Figures 2(a) and 2(b) show the Fe film on ferroelectric $BaTiO_3$ substrate with in-plane and out-of-plane polarization domains, exhibiting uniaxial and cubic magnetic anisotropy [34]. In the simulation, a $6000 \times 400 \times 2$ nm^3 Fe film is discretized using $3000 \times 200 \times 1$ finite difference cells. The periodic boundary condition is used along the y axis to avoid the boundary effect. The simulation parameters used are as follows [23,35]: saturation magnetization $M_s = 1.7 \times 10^6$ A/m, exchange constant $A_{ex} = 2.1 \times 10^{-11}$ J/m, Gilbert damping $\alpha = 0.003$, cubic anisotropy constant $K_c = 4.4 \times 10^4$ J/m^3, and uniaxial anisotropy constant $K_u = 1.5 \times 10^4$ J/m^3. To prevent SW reflection at both ends, α is gradually increased from 0.003 to 0.033 at both end regions of the Fe film (-3000 nm $< x < -2200$ nm, 2200 nm $< x <$ 3000 nm). An external magnetic field $\mu_0 H_{ext} = 100$ mT is applied to magnetize the Fe film along the y axis. To obtain the dispersion relation of SWs, we perform two-dimensional Fourier transform [46,47] on $m_x(x,t)$ in response to a sinc-based exciting field $h_0 \mathrm{sinc}(2\pi f_c(t-t_0))\hat{e}_x$ with $\mu_0 h_0 =$ 10 mT, cutoff frequency $f_c = 50$ GHz and $t_0 = 5$ ns, at the center section ($6 \times 400 \times 2$ nm^3) of Fe film. The dispersion relations are shown in Figs. 2(c) and 2(d) for cubic and uniaxial regions, respectively. The red dashed lines represent the theoretical calculations from the dispersion relation equations of Damon-Eshbach (DE) SWs in cubic and uniaxial anisotropy regions as follows [24,48]:

$$f_{cu} = F_{cu}(k), = \frac{\gamma\mu_0}{2\pi}\sqrt{\left(H_{ext} - \frac{2K_c}{\mu_0 M_s} + \frac{2A_{ex}}{\mu_0 M_s}k^2\right)\left(H_{ext} + \frac{K_c}{\mu_0 M_s} + M_s + \frac{2A_{ex}}{\mu_0 M_s}k^2\right) + M_s^2 F}, \tag{5}$$

$$f_{ku} = F_{ku}(k), = \frac{\gamma\mu_0}{2\pi}\sqrt{\left(H_{ext} + \frac{2K_u}{\mu_0 M_s} + \frac{2A_{ex}}{\mu_0 M_s}k^2\right)\left(H_{ext} + \frac{2K_u}{\mu_0 M_s} + M_s + \frac{2A_{ex}}{\mu_0 M_s}k^2\right) + M_s^2 F}, \tag{6}$$

where, γ is gyromagnetic ratio, μ_0 is vacuum permeability, $F = (1 - e^{-|k|d})/|k|d\{1 - [(1 - e^{-|k|d})/|k|d]\}$, d is the thickness of Fe film. Obviously, the variance in anisotropy constants between uniaxial and cubic regions yields distinct dispersion relations.

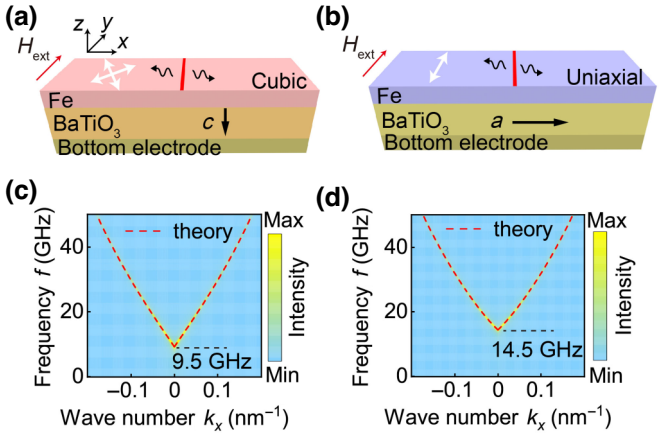

FIG. 2. (a) The cubic anisotropy is induced in Fe layer on ferroelectric $BaTiO_3$ c domain. The two white double-head arrows represent easy axes of cubic anisotropy along with 45° to the y axis. (b) The uniaxial anisotropy is induced in Fe layer on ferroelectric $BaTiO_3$ a domain. The white double-head arrows represent the easy axis of uniaxial anisotropy along the y axis. The image plots of the dispersion relation of SWs in the cubic anisotropy region (c) and uniaxial anisotropy region (d) by micromagnetic simulation. The dashed lines correspond to the theory calculation data.

We then simulate the reflection and transmission of SWs by moving MAB, as depicted in Fig. 3(a). The exciting source of SWs is 1.478 μm from the left end with a size of $42 \times 400 \times 2$ nm^3. The SW is excited by a consistent Sine function field $\mu_0 h_0 \sin(2\pi f_0 t)\hat{e}_x$ ($\mu_0 h_0 = 10$ mT, $f_0 = 20$ GHz) under the external magnetic field $\mu_0 H_{ext} =$ 100 mT. The excited SW propagates in Fe film along the x axis perpendicular to the MAB. The width of MAB, the same as the pinned ferroelectric domain wall (2–5 nm [49–51]), is far smaller than the wavelength of SWs and we neglect it in simulation by setting the abruptly changed anisotropy between two different cells. The MAB moves along the x axis between $x = -1100$ nm and $x = 1900$ nm marked by the blue dash lines in Fig. 3(a). It has been confirmed that the velocity of the ferroelectric domain wall driven by electric field can be up to 1000 m/s in $BaTiO_3$ [52,53]. And, the velocity of MAB (v_{MAB}) could be calculated by the Miller-Weinreich theory as per the following equation [52,54]:

$$v_{MAB}(U) = v_\infty \sum_{n=1}^{\infty} n e^{-(\delta/(U/D))n^{\frac{3}{2}}}, \tag{7}$$

where U is the voltage to provide perpendicular electric field in $BaTiO_3$, $v_\infty = 5$ m/s, $\delta = 4$ kV/cm, the thickness of $BaTiO_3$ substrate $D = 100$ nm, n is the positive integer. So, a significant velocity of MAB could be realized by a much lower voltage.

In the simulation, we implement MAB moving at velocity v_{MAB} by shifting it over one discretization cell

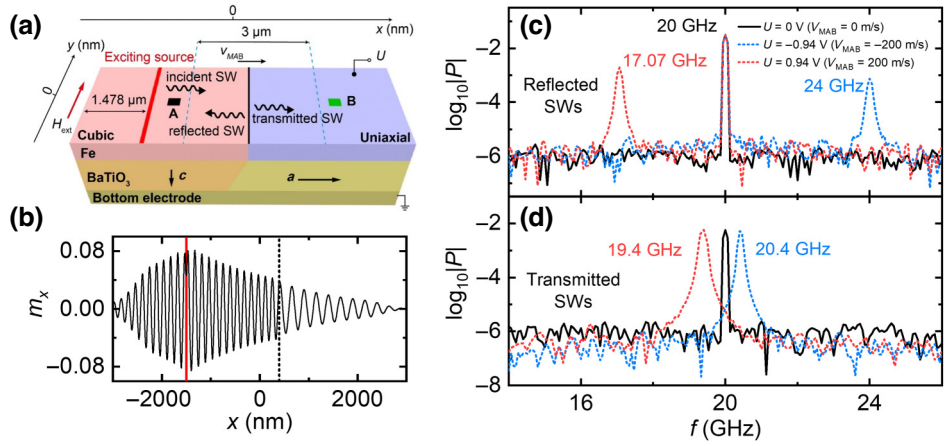

FIG. 3. (a) The schematic of reflected and transmitted SWs by moving MAB with voltage. The MAB moves along the x axis between -1100 nm and 1900 nm marked by the blue dash lines. The black square (A) represents the cell at -1202 nm $< x < -1200$ nm, -2 nm $< y < 0$ nm, where $m_x(t)$ is recorded as the incident and reflected SWs. The green square (B) represents the cell at 1998 nm $< x < 2000$ nm, -2 nm $< y < 0$ nm, where $m_x(t)$ is recorded as the transmitted SW. (b) The snapshot of m_x taken at $y = -1$ nm with the static MAB at $x = 400$ nm. The red line is the position of exciting source and the black dashed line is the position of MAB. (c) The spectra of reflected and incident SWs when $v_{\mathrm{MAB}} = -200$, 0 and 200 m/s. (d) The spectra of transmitted SW when $v_{\mathrm{MAB}} = -200$, 0 and 200 m/s.

($\delta x = 2$ nm) every time interval $\delta t = \delta x / v_{\mathrm{MAB}}$ [35,55]. The m_x in the cell of -1202 nm $< x < -1200$ nm, -2 nm $< y < 0$ nm is recorded as incident and reflected SWs, while the m_x in the cell of 1998 nm $< x < 2000$ nm, -2 nm $< y < 0$ nm is recorded as transmitted SW, marked by the black and green squares A, B in Fig. 3(a), respectively. Figure 3(b) shows the snapshot of m_x taken at $y = -1$ nm with static MAB at $x = 400$ nm. The black dashed line indicates the position of MAB. Clearly, the SWs have different wavelengths in cubic and uniaxial regions. To accurately determine all the related frequencies of the SWs, we perform a fast Fourier transform on $m_x(t)$ at A and B to obtain the spectra of reflected and transmitted SWs. Figure 3(c) shows the spectra of the incident and reflected SWs at various v_{MAB}. At $v_{\mathrm{MAB}} = 0$ m/s, a single 20-GHz peak in the spectrum (black solid curve) indicates the reflected SW frequency matches exciting frequency. However, for $v_{\mathrm{MAB}} = 200$ m/s, the spectrum (red dashed curve) displays peaks at 20 and 17.07 GHz. The latter peak, the reflected SW, shows a significant red shift of the Doppler effect. With a negative voltage setting $v_{\mathrm{MAB}} = -200$ m/s, reflected SW frequency blue shifts to 24 GHz. Figure 3(d) shows the spectra of transmitted SW for various MAB velocities. They all have a single peak due to the solitary transmitted spin wave in the B. The transmitted SW frequencies display a Doppler red shift to 19.4 GHz and blue shift to 20.4 GHz at $v_{\mathrm{MAB}} = 200$ and -200 m/s, respectively. Notably, these Doppler shifts are much lower than those of the reflected SWs, which hold opposing wave vectors to the incident SW.

To comprehensively analyze the Doppler shift, we simulate the SW Doppler shift across a broader range of velocities (voltages). Figure 4(a) plots both simulated and theoretical Doppler shifts of reflected and transmitted SWs' frequencies at the exciting frequency of 20 GHz in the cubic region. The simulation aligns closely with theoretical predictions. The frequencies of reflected and transmitted SWs show a monotonic shift with the velocity (voltage). This also means all the reflected and transmitted SWs show a red shift when the MAB is far away from the source of the SW. Meanwhile, the SWs show a blue shift when the MAB is close to the SW source. In addition, the SW Doppler shift can exceed several GHz, nearly two orders greater than the electric current control methods. It is also interesting the transmission SW shows a different velocity-dependent tendency when the incident SW from uniaxial region to cubic region shown in Fig. 4(b). Here, the transmitted SWs show a blue shift when the MAB is far away from the SW source, and a red shift when the MAB is close to the source. Such unusual Doppler shift comes from the negative value of $\mathbf{k}_0 - \mathbf{k}_t'$ based on Eq. (4). These results also indicate that the type of transmitted SW Doppler shift is influenced not only by the MAB's movement direction but also by the deviation between the two different regions.

In summary, we predict an efficient way to control the SW Doppler shift by voltage-control MAB movement in the FM-FE heterojunction. The SW Doppler shift could be modulated in an ultra-wide-band range with voltage. The micromagnetic simulation results align closely with theoretical predictions. Such a significant SW Doppler shift could be employed as an accurate probe of the ferroelectric domain-wall motion controlled by electric field. On the other hand, if the velocity of magnetic domain-wall

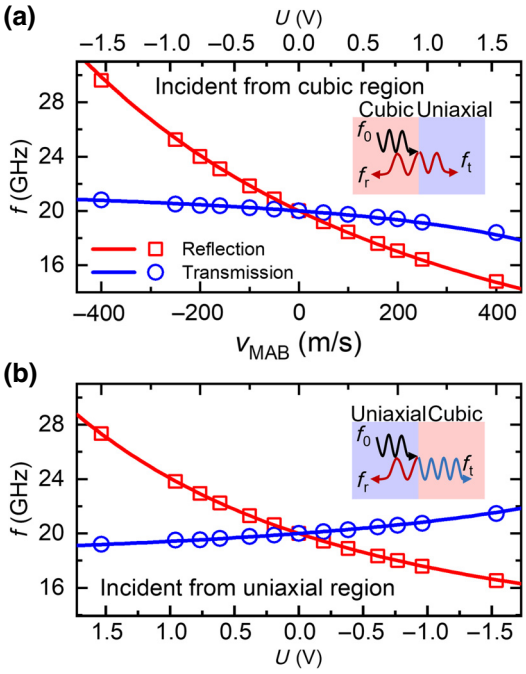

FIG. 4. The frequencies of reflected and transmitted SWs as a function v_{MAB} (voltage) in $Fe/BiTiO_3$ at the exciting frequency of 20 GHz. (a) The SWs incident from cubic to uniaxial region. The positive voltage provides the positive velocity of MAB. (b) The SWs incident from uniaxial to the cubic regions. The negative voltage provides the positive velocity of MAB. The symbols are corresponding to the simulation results. The solid lines correspond to the theoretical calculation.

motion surpasses the maxium spin-wave group velocity of the magnetic material system, it will trigger a phenomenon reminiscent of a spin-wave black hole at the boundary. Employing ultrafast optical techniques to investigate the propagation dynamics of spin waves may provide one possible way for doing analogue gravity and measuring the Hawking radiation of an analogue black hole.

ACKNOWLEDGMENTS

This work is partially supported by National JSPS Program for Grant-in-Aid for Scientific Research (S) (Grant No. 21H05021), and Challenging Exploratory Research (Grant No. 17H06227) and JST CREST (Grant No. JPMJCR18J1). Natural Science Foundation of Shaanxi Province (Grant No. 2021JM-022).

[1] Sebastian Neusser and Dirk Grundler, Magnonics: Spin waves on the nanoscale, Adv. Mater. **21**, 2927 (2009).
[2] V. V. Kruglyak, S. O. Demokritov, and D. Grundler, Magnonics, J. Phys. D: Appl. Phys. **43**, 260301 (2010).
[3] A. A. Serga, A. V. Chumak, and B. Hillebrands, YIG magnonics, J. Phys. D: Appl. Phys. **43**, 264002 (2010).
[4] B. Lenk, H. Ulrichs, F. Garbs, and M. Münzenberg, The building blocks of magnonics, Phys. Rep. **507**, 107 (2011).
[5] Sergej O. Demokritov and Andrei N. Slavin, *Magnonics: From Fundamentals to Applications* (Springer Science & Business Media, Heidelberg, 2012), Vol. 125.
[6] Anjan Barman, Gianluca Gubbiotti, Sam Ladak, Adekunle Olusola Adeyeye, Maciej Krawczyk, Joachim Gräfe, Christoph Adelmann, Sorin Cotofana, Azad Naeemi, Vitaliy I. Vasyuchka, *et al.*, The 2021 magnonics roadmap, J. Phys.: Condens. Matter **33**, 413001 (2021).
[7] Philipp Pirro, Vitaliy I. Vasyuchka, Alexander A. Serga, and Burkard Hillebrands, Advances in coherent magnonics, Nat. Rev. Mater. **6**, 1114 (2021).
[8] M. P. Kostylev, A. A. Serga, T. Schneider, B. Leven, and B. Hillebrands, Spin-wave logical gates, Appl. Phys. Lett. **87**, 153501 (2005).
[9] Ki-Suk Lee and Sang-Koog Kim, Conceptual design of spin wave logic gates based on a Mach–Zehnder-type spin wave interferometer for universal logic functions, J. Appl. Phys. **104**, 053909 (2008).
[10] S. Klingler, P. Pirro, T. Brächer, B. Leven, B. Hillebrands, and A. V. Chumak, Design of a spin-wave majority gate employing mode selection, Appl. Phys. Lett. **105**, 152410 (2014).
[11] B. Dieny, *et al.*, Opportunities and challenges for spintronics in the microelectronics industry, Nat. Electron. **3**, 446 (2020).
[12] Daniel D. Stancil, Benjamin E. Henty, Ahmet G. Cepni, and J. P. Van't Hof, Observation of an inverse Doppler shift from left-handed dipolar spin waves, Phys. Rev. B **74**, 060404 (2006).
[13] Vincent Vlaminck and Matthieu Bailleul, Current-induced spin-wave Doppler shift, Science **322**, 410 (2008).
[14] Hong Xia, Jie Chen, Xiaoyan Zeng, and Ming Yan, Doppler effect in a solid medium: Spin wave emission by a precessing domain wall drifting in spin current, Phys. Rev. B **93**, 140410 (2016).
[15] Tao Yu, Chen Wang, Michael A. Sentef, and Gerrit E. W. Bauer, Spin-wave Doppler shift by magnon drag in magnetic insulators, Phys. Rev. Lett. **126**, 137202 (2021).
[16] Jotaro J. Nakane and Hiroshi Kohno, Current-induced spin-wave Doppler shift in antiferromagnets, J. Phys. Soc. Jpn. **90**, 103705 (2021).
[17] Gil Jannes, Philippe Maïssa, Thomas G. Philbin, and Germain Rousseaux, Hawking radiation and the boomerang behavior of massive modes near a horizon, Phys. Rev. D **83**, 104028 (2011).
[18] A. Roldán-Molina, Alvaro S. Nunez, and R. A. Duine, Magnonic black holes, Phys. Rev. Lett. **118**, 061301 (2017).
[19] M. Balinskiy, A. C. Chavez, A. Barra, H. Chiang, G. P. Carman, and A. Khitun, Magnetoelectric spin wave modulator based on synthetic multiferroic structure, Sci. Rep. **8**, 10867 (2018).
[20] A. V. Sadovnikov, A. A. Grachev, S. E. Sheshukova, Y. P. Sharaevskii, A. A. Serdobintsev, D. M. Mitin, and S. A. Nikitov, Magnon straintronics: Reconfigurable spin-wave routing in strain-controlled bilateral magnetic stripes, Phys. Rev. Lett. **120**, 257203 (2018).

[21] Bivas Rana and YoshiChika Otani, Voltage-controlled reconfigurable spin-wave nanochannels and logic devices, Phys. Rev. Appl. **9**, 014033 (2018).
[22] Bivas Rana and YoshiChika Otani, Towards magnonic devices based on voltage-controlled magnetic anisotropy, Commun. Phys. **2**, 90 (2019).
[23] Huajun Qin, Rouven Dreyer, Georg Woltersdorf, Tomoyasu Taniyama, and Sebastiaan van Dijken, Electric-field control of propagating spin waves by ferroelectric domain-wall motion in a multiferroic heterostructure, Adv. Mater. **33**, 2100646 (2021).
[24] Kang Wang, Shaojie Hu, Fupeng Gao, Miaoxin Wang, and Dawei Wang, Dual function spin-wave logic gates based on electric field control magnetic anisotropy boundary, Appl. Phys. Lett. **120**, 142405 (2022).
[25] Sarbeswar Sahoo, Srinivas Polisetty, Chun-Gang Duan, Sitaram S. Jaswal, Evgeny Y. Tsymbal, and Christian Binek, Ferroelectric control of magnetism in $BaTiO_3$/ Fe heterostructures via interface strain coupling, Phys. Rev. B **76**, 092108 (2007).
[26] G. Venkataiah, Y. Shirahata, I. Suzuki, M. Itoh, and T. Taniyama, Strain-induced reversible and irreversible magnetization switching in $Fe/BaTiO_3$ heterostructures, J. Appl. Phys. **111**, 033921 (2012).
[27] Tuomas H. E. Lahtinen, Yasuhiro Shirahata, Lide Yao, Kévin J. A. Franke, Gorige Venkataiah, Tomoyasu Taniyama, and Sebastiaan van Dijken, Alternating domains with uniaxial and biaxial magnetic anisotropy in epitaxial Fe films on $BaTiO_3$, Appl. Phys. Lett. **101**, 262405 (2012).
[28] G. Venkataiah, E. Wada, H. Taniguchi, M. Itoh, and T. Taniyama, Electric-voltage control of magnetism in $Fe/BaTiO_3$ heterostructured multiferroics, J. Appl. Phys. **113**, 17C701 (2013).
[29] Venkataiah Gorige, Anupama Swain, Katsuyoshi Komatsu, Mitsuru Itoh, and Tomoyasu Taniyama, Magnetization reversal in $Fe/BaTiO_3$ (110) heterostructured multiferroics, Phys. Status Solidi RRL **11**, 1700294 (2017).
[30] S. Yamada, Y. Teramoto, D. Matsumi, D. Kepaptsoglou, I. Azaceta, T. Murata, K. Kudo, V. K. Lazarov, T. Taniyama, and K. Hamaya, Electric field tunable anisotropic magnetoresistance effect in an epitaxial $Co_2FeSi/BaTiO_3$ interfacial multiferroic system, Phys. Rev. Mater. **5**, 014412 (2021).
[31] T. Usami, S. Fujii, S. Yamada, Y. Shiratsuchi, R. Nakatani, and K. Hamaya, Giant magnetoelectric effect in an L21-ordered $Co_2FeSi/Pb(Mg_1/3Nb_2/3)O_3$-$PbTiO_3$ multiferroic heterostructure, Appl. Phys. Lett. **118**, 142402 (2021).
[32] Shumpei Fujii, Takamasa Usami, Yu Shiratsuchi, Adam M. Kerrigan, Amran Mahfudh Yatmeidhy, Shinya Yamada, Takeshi Kanashima, Ryoichi Nakatani, Vlado K. Lazarov, Tamio Oguchi, *et al.*, Giant converse magnetoelectric effect in a multiferroic heterostructure with polycrystalline Co_2FeSi, NPG Asia Mater. **14**, 43 (2022).
[33] Shaojie Hu, Shinya Yamada, Po-Chun Chang, Wen-Chin Lin, Kohei Hamaya, and Takashi Kimura, Efficient electrical manipulation of the magnetization process in an epitaxially controlled $Co_2FeSi/BaTiO_3$ multiferroic interface, Phys. Rev. Appl. **20**, 034029 (2023).
[34] Tuomas H. E. Lahtinen, Yasuhiro Shirahata, Lide Yao, Kévin J. A. Franke, Gorige Venkataiah, Tomoyasu Taniyama, and Sebastiaan van Dijken, Alternating domains with uniaxial and biaxial magnetic anisotropy in epitaxial Fe films on $BaTiO_3$, Appl. Phys. Lett. **101**, 262405 (2012).
[35] Kévin J. A. Franke, Ben Van de Wiele, Yasuhiro Shirahata, Sampo J. Hämäläinen, Tomoyasu Taniyama, and Sebastiaan van Dijken, Reversible electric-field-driven magnetic domain-wall motion, Phys. Rev. X **5**, 011010 (2015).
[36] M. B. Fogel, S. E. Trullinger, A. R. Bishop, and J. A. Krumhansl, Dynamics of Sine-Gordon solitons in the presence of perturbations, Phys. Rev. B **15**, 1578 (1977).
[37] John David Jackson, *Classical Electrodynamics* (John Wiley & Sons, New York, 2021), Chapter 11.
[38] F. Duncan M. Haldane, Nonlinear field theory of large-spin heisenberg antiferromagnets: Semiclassically quantized solitons of the one-dimensional easy-axis Néel state, Phys. Rev. Lett. **50**, 1153 (1983).
[39] Se Kwon Kim, Yaroslav Tserkovnyak, and Oleg Tchernyshyov, Propulsion of a domain wall in an antiferromagnet by magnons, Phys. Rev. B **90**, 104406 (2014).
[40] Olena Gomonay, Tomas Jungwirth, and Jairo Sinova, High antiferromagnetic domain wall velocity induced by Néel spin-orbit torques, Phys. Rev. Lett. **117**, 017202 (2016).
[41] Takayuki Shiino, Se-hyeok Oh, Paul M. Haney, Seo-won Lee, Gyungchoon Go, Byong-Guk Park, and Kyung-Jin Lee, Antiferromagnetic domain wall motion driven by spin-orbit torques, Phys. Rev. Lett. **117**, 087203 (2016).
[42] Lucas Caretta, Se-Hyeok Oh, Takian Fakhrul, Dong-Kyu Lee, Byung Hun Lee, Se Kwon Kim, Caroline A. Ross, Kyung-Jin Lee, and Geoffrey S. D. Beach, Relativistic kinematics of a magnetic soliton, Science **370**, 1438 (2020).
[43] Chun-Gang Duan, S. S. Jaswal, and E. Y. Tsymbal, Predicted magnetoelectric effect in $Fe/BaTiO_3$ multilayers: Ferroelectric control of magnetism, Phys. Rev. Lett. **97**, 047201 (2006).
[44] G. Radaelli, D. Petti, E. Plekhanov, I. Fina, P. Torelli, B. R. Salles, M. Cantoni, C. Rinaldi, D. Gutiérrez, G. Panaccione, M. Varela, S. Picozzi, J. Fontcuberta, and R. Bertacco, Electric control of magnetism at the $Fe/BaTiO_3$ interface, Nat. Commun. **5**, 3404 (2014).
[45] Arne Vansteenkiste, Jonathan Leliaert, Mykola Dvornik, Mathias Helsen, Felipe Garcia-Sanchez, and Bartel Van Waeyenberge, The design and verification of MuMax3, AIP. Adv. **4**, 107133 (2014).
[46] Dheeraj Kumar, Oleksandr Dmytriiev, Sabareesan Ponraj, and Anjan Barman, Numerical calculation of spin wave dispersions in magnetic nanostructures, J. Phys. D: Appl. Phys. **45**, 015001 (2011).
[47] G. Venkat, D. Kumar, M. Franchin, O. Dmytriiev, M. Mruczkiewicz, H. Fangohr, A. Barman, M. Krawczyk, and A. Prabhakar, Proposal for a standard micromagnetic problem: Spin wave dispersion in a magnonic waveguide, IEEE Trans. Magn. **49**, 524 (2013).
[48] B. A. Kalinikos and A. N. Slavin, Theory of dipole-exchange spin wave spectrum for ferromagnetic films with mixed exchange boundary conditions, J. Phys. C: Solid State Phys. **19**, 7013 (1986).
[49] X. Zhang, T. Hashimoto, and D. C. Joy, Electron holographic study of ferroelectric domain walls, Appl. Phys. Lett. **60**, 784 (1992).

[50] J. Hlinka and P. Márton, Phenomenological model of a 90° domain wall in $BaTiO_3$-type ferroelectrics, Phys. Rev. B **74**, 104104 (2006).

[51] Qingsong Zhang and William A. Goddard, Charge and polarization distributions at the 90° domain wall in barium titanate ferroelectric, Appl. Phys. Lett. **89**, 182903 (2006).

[52] H. L. Stadler and P. J. Zachmanidis, Nucleation and growth of ferroelectric domains in $BaTiO_3$ at fields from 2 to 450 kV/cm, J. Appl. Phys. **34**, 3255 (1963).

[53] V. Boddu, F. Endres, and P. Steinmann, Molecular dynamics study of ferroelectric domain nucleation and domain switching dynamics, Sci. Rep. **7**, 806 (2017).

[54] Alexander Kirillovich Tagantsev, L. Eric Cross, and Jan Fousek, *Domains in Ferroic Crystals and Thin Films* (Springer, New York, 2010), Vol. 13.

[55] Ben Van de Wiele, Jonathan Leliaert, Kévin J. A. Franke, and Sebastiaan van Dijken, Electric-field-driven dynamics of magnetic domain walls in magnetic nanowires patterned on ferroelectric domains, New J. Phys. **18**, 033027 (2016).